Uncertainty quantification in rock physics full waveform inversion

Qi Hu, Tianze Zhang, and Kristopher A. Innanen

ABSTRACT

Uncertainty quantification is a fundamental aspect of seismic analysis, enhancing the reliability of results obtained from seismic data. This practice enables a more informed and responsible approach to decision-making in various engineering and geoscience applications. We establish a recurrent neural network with rules that enforce the integration of rock physics modeling and elastic wave propagation. The network is then trained using the wavefield projected onto a measurement surface as labeled data, which is compared with observed seismic data. This training process involves the direct prediction of rock physics properties through Full Waveform Inversion (FWI). Utilizing the Automatic Differential method, we accurately and efficiently construct gradients through inspection and the use of the computational graph. The inverse Hessian, closely related to the posterior covariance operator, is then approximated using these gradients, providing uncertainty estimations for the rock physics variables. Our workflow is applied to address two geophysical inverse problems: seismic reservoir characterization and time-lapse CO_2 monitoring.

INTRODUCTION

The retrieval of physical properties of the earth using seismic data has been subject to intensive research for the last decades (Aki and Richards, 2002; Sen, 2006; Menke, 2018). In parallel, because of the increase in computational power, complex forward modeling has become more affordable. One of the methods that potentially allows to extract more information from seismic data is Full Waveform Inversion (FWI) (Tarantola, 1986; Pratt et al., 1998; Virieux and Operto, 2009). In FWI an attempt is made to construct elastic models of the subsurface matching not only arrival times and amplitudes, but the full amplitude and phase information of the measured waveform data. Theoretically, it can provide models of physical parameters with a higher spatial resolution than other methods such as travel-time tomography (Schuster, 2017).

Reservoir characterization usually requires integrating different types of data. The uncertainty associated with this process comes from several sources: measurement errors in seismic and well-log data, data processing, approximate wave propagation model, and the rock physics transformation from elastic properties to reservoir properties. One fundamental reason for quantifying uncertainty is to report error bars along with interpretation results. A more practical reason is for risk analysis and optimal decision-making (Bosch et al., 2010). For an inverse problem, when quantifying uncertainty a user seeks to determine the posterior probability distribution of model variables conditioned on the measured data. Due to the high dimensionality of the model space paired with the computational costs of the forward problem, stochastic methods such as Monte Carlo are generally infeasible for FWI, causing the development of uncertainty quantification in FWI lagged considerably behind. Most proposed approaches in this area are based on low-rank estimates of the posterior covariance matrix, for example, the inverse Hessian (Bui-Thanh et al., 2013; Liu

and Peter, 2019). New approaches are also emerging (Gebraad et al., 2020; Keating and Innanen, 2021).

THEORY

Forward modeling

The forward operator for the prediction of the seismic response includes a rock physics model that maps rock and fluid properties (e.g., porosity, mineral volumes, and fluid saturations) to elastic properties (e.g., P- and S-wave velocity, and density) and a wave propagation model that computes seismic data. The general forward model is expressed symbolically as follows

$$\mathbf{d}_{\text{seis}} = f_{\text{seis}}(f_{\text{rpm}}(\mathbf{m_r})) + \mathbf{e}, \tag{1}$$

where the rock physics relation f_{rpm} in our study is based on granular media theory and Gaussian's equation (Mavko et al., 2020); the wave propagation model f_{seis} we consider is isotropic-elastic wave equations. The seismic data $\mathbf{d}_{\text{seis}}$ are in terms of particle velocities, $\mathbf{m_r}$ are rock physics properties, and $\mathbf{e}$ are data errors.

RNN-FWI

Conventional seismic Full Waveform Inversion (FWI) is a complex data-fitting procedure aimed at extracting essential information from seismic records. The key components include an efficient forward modeling method for simulating synthetic data and a descent-based local optimization method for updating the model (Tarantola, 1986; Virieux and Operto, 2009). In general, FWI is designed to determine elastic properties, from which the rock properties of interest can be derived. The rock physics FWI approach by Hu et al. (2021) allows direct inversion of seismic data for rock properties and shares the same numerical structure as conventional elastic FWI.

Studies by (Sun et al., 2020; Zhang et al., 2020) have demonstrated the effective simulation of seismic wave propagation using a specialized recurrent neural network (RNN). Importantly, it has been shown that the training process of such a network is equivalent to performing FWI. At the heart of RNN-FWI is the Automatic Differentiation method, facilitating the construction of gradients through inspection and utilization of the computational graph. This observation motivates us to extend the analysis of RNN-FWI beyond those previously explored. For instance, we aim to delve into the complexities of the multi-physics inverse problem, as represented in Equation 1.

Relation of Hessian to the posterior covariance

According to Bayesian inference, the solution to an inverse problem yields the posterior probability density, which is defined as

$$P(\mathbf{m}|\mathbf{d}_{\text{obs}}) \propto P(\mathbf{d}_{\text{obs}}|\mathbf{m})\mathbf{P}(\mathbf{m}), \tag{2}$$

where $P(\mathbf{d}_{\text{obs}}|\mathbf{m})$ is the likelihood and $P(\mathbf{m})$ is prior probability density. Assuming Gaussian noise with zero mean and covariance $\mathbf{C}_d^{-1}$, and Gaussian prior with center $\mathbf{m}_{\text{prior}}$ and

covariance $\mathbf{C}_m^{-1}$, equation 2 is then

$$P(\mathbf{m}|\mathbf{d}_{\text{obs}}) \propto \exp(-S(\mathbf{m})), \tag{3}$$

where $S(\mathbf{m})$ is the misfit function:

$$2\ S(\mathbf{m}) = (\mathbf{d}_{\text{obs}} - \mathbf{g}(\mathbf{m}))^t \mathbf{C}_d^{-1} (\mathbf{d}_{\text{obs}} - \mathbf{g}(\mathbf{m})) + (\mathbf{m} - \mathbf{m}_{\text{prior}})^t \mathbf{C}_m^{-1} (\mathbf{m} - \mathbf{m}_{\text{prior}}), \tag{4}$$

If the equation $\mathbf{d} = \mathbf{g}(\mathbf{m})$ solving the forward problem is linear, i.e., $\mathbf{d} = \mathbf{G}\mathbf{m}$, the misfit function is quadratic in $\mathbf{m}$, and the posterior probability is also Gaussian (Tarantola, 2005):

$$P(\mathbf{m}|\mathbf{d}_{\text{obs}}) \propto \exp\left(-\frac{1}{2}(\mathbf{m} - \hat{\mathbf{m}})^t \mathbf{C}_M^{-1} (\mathbf{m} - \hat{\mathbf{m}})\right), \tag{5}$$

with the posterior mean and covariance matrix given by

$$\hat{\mathbf{m}} = \mathbf{m}_{\text{prior}} + (\mathbf{G}^t \mathbf{C}_d^{-1} \mathbf{G} + \mathbf{C}_m^{-1})^{-1} \mathbf{G}^t \mathbf{C}_d^{-1} (\mathbf{d}_{\text{obs}} - \mathbf{G}\mathbf{m}_{\text{prior}}), \tag{6}$$

and

$$\mathbf{C}_M = (\mathbf{G}^t \mathbf{C}_d^{-1} \mathbf{G} + \mathbf{C}_m^{-1})^{-1}, \tag{7}$$

If $\mathbf{g}(\mathbf{m})$ is not a linear function of $\mathbf{m}$, $P(\mathbf{m}|\mathbf{d}_{\text{obs}})$ is not Gaussian. One simplistic approach is to linearize the forward operator around the maximum a posteriori model $\mathbf{m}_{\text{MAP}}$:

$$\mathbf{g}(\mathbf{m}) = \mathbf{g}(\mathbf{m}_{\text{MAP}}) + \tilde{\mathbf{G}}(\mathbf{m} - \mathbf{m}_{\text{MAP}}), \tag{8}$$

where $\tilde{\mathbf{G}} = \frac{\partial \mathbf{g}(\mathbf{m})}{\partial \mathbf{m}}$ is the Fréchet derivative. As the MAP solution is the point minimizing the misfit function in equation 4, we face here the typical problem of nonlinear least-squares minimization. Using, for instance, RNN-FWI to update the model until convergence, we obtain $\mathbf{m}_{\text{MAP}}$ and then use a linearization of $\mathbf{g}(\mathbf{m})$ around $\mathbf{m}_{\text{MAP}}$ to estimate the posterior covariance:

$$\mathbf{C}_M = (\tilde{\mathbf{G}}^t \mathbf{C}_d^{-1} \tilde{\mathbf{G}} + \mathbf{C}_m^{-1})^{-1} = (\mathbf{H}_d + \mathbf{C}_m^{-1})^{-1}, \tag{9}$$

where $\mathbf{H}_d = \tilde{\mathbf{G}}^t \mathbf{C}_d^{-1} \tilde{\mathbf{G}}$ is the Gauss-Newton approximation of the data misfit Hessian.

The most trivial use of the posterior covariance matrix $\mathbf{C}_M$ is to interpret the square roots of the diagonal elements (variance) as 'uncertainty bars' on the estimated model parameters, and the comparison of these posterior uncertainties with the prior uncertainties (as represented by $\mathbf{C}_m$) shows which parameters have been resolved and by how much.

NUMERICAL EXAMPLES

Reservoir characterization

To investigate the multi-physics RNN-FWI approach for characterizing hydrocarbon units, we introduce a geologically realistic reservoir model, focusing on a selected section of the elastic Marmousi2 model (see Figure 1). The model spans 2 km in width, 2 km in depth, with a grid spacing of 20 m. In this model, we assign rock physics properties to each cell, assuming a rock frame comprising quartz and clay saturated with water and gas. This

results in three model unknowns: porosity, clay content, and water saturation. Notably, a gas sand trap is incorporated into the model, situated at a depth of 0.76 km and laterally positioned at 0.8 km. This gas sand trap is characterized by a higher porosity of 0.3, a lower clay content of 0.15, and a reduced water saturation of 0.35.

We adopt an acquisition geometry employing receivers that mimic a simultaneous surface seismic and vertical seismic profile (VSP) configuration. Specifically, there are a total of 10 evenly distributed sources at the top of the model, illuminating receivers on both the top and sides of the model. The initial rock property models are smoothed versions of the true models.

Our high-resolution inversion results reveal the accurate depiction of relevant reservoir structures, allowing for the identification of the gas sand within the recovered models. Figure 2 presents an examination of absolute errors and standard deviations for these recovered models. Our criterion for successful uncertainty quantification is that the standard deviation should align well with the absolute model error. In this context, the estimated uncertainty proves satisfactory. Furthermore, the uncertainty results exhibit a strong correlation with the expected sensitivity of the rock physics variables. Porosity, being the most sensitive, displays the smallest uncertainty, while saturation, being the least sensitive, exhibits the overall largest uncertainty. In Figure 3, the velocity and density models corresponding the true and inverted rock property models are plotted. The true models are accurately recovered, with relatively larger uncertainties observed around the gas trap. Figure 4 illustrates the success of our inversion in reproducing the seismic data.

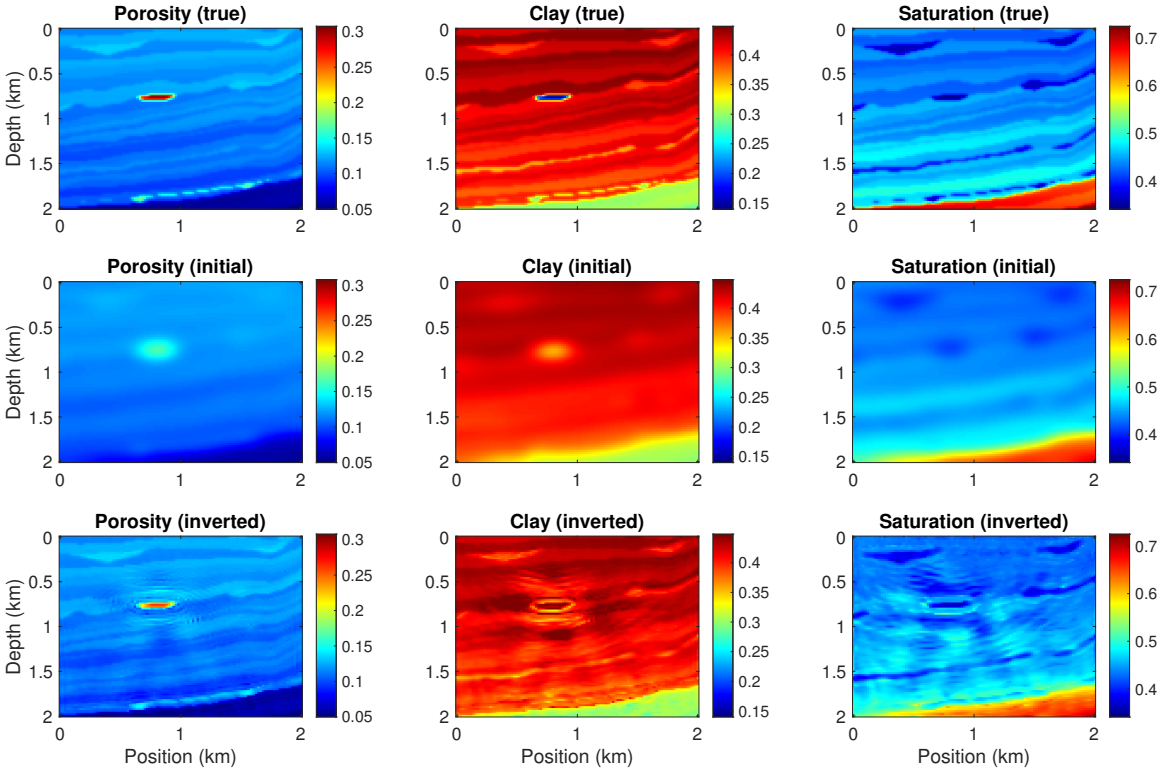

FIG. 1. True, initial, and inverted models of porosity, clay content, and water saturation.

.

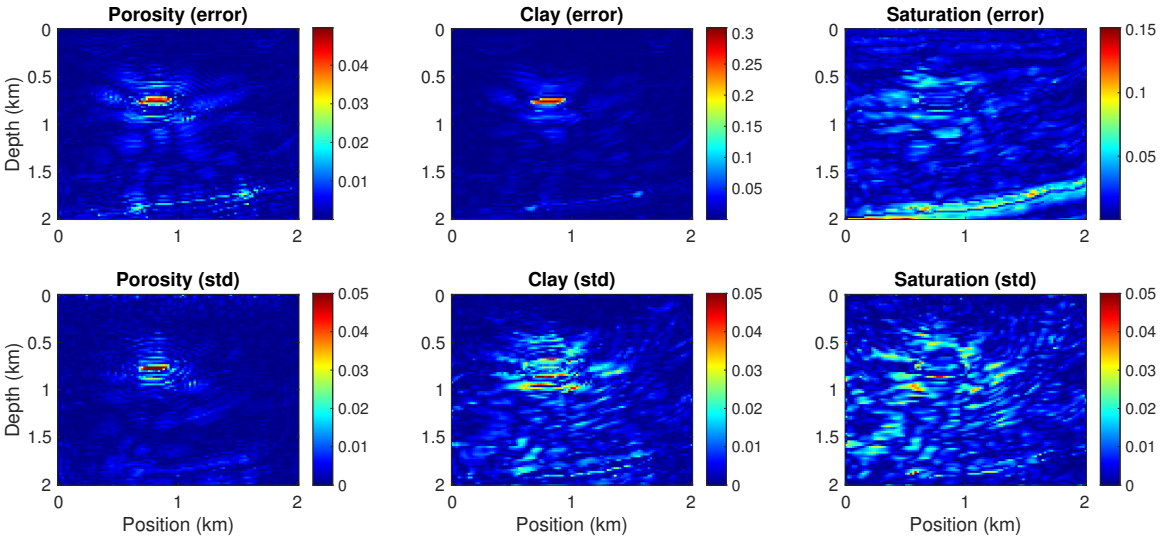

FIG. 2. Errors and standard deviations for the inverted models.

.

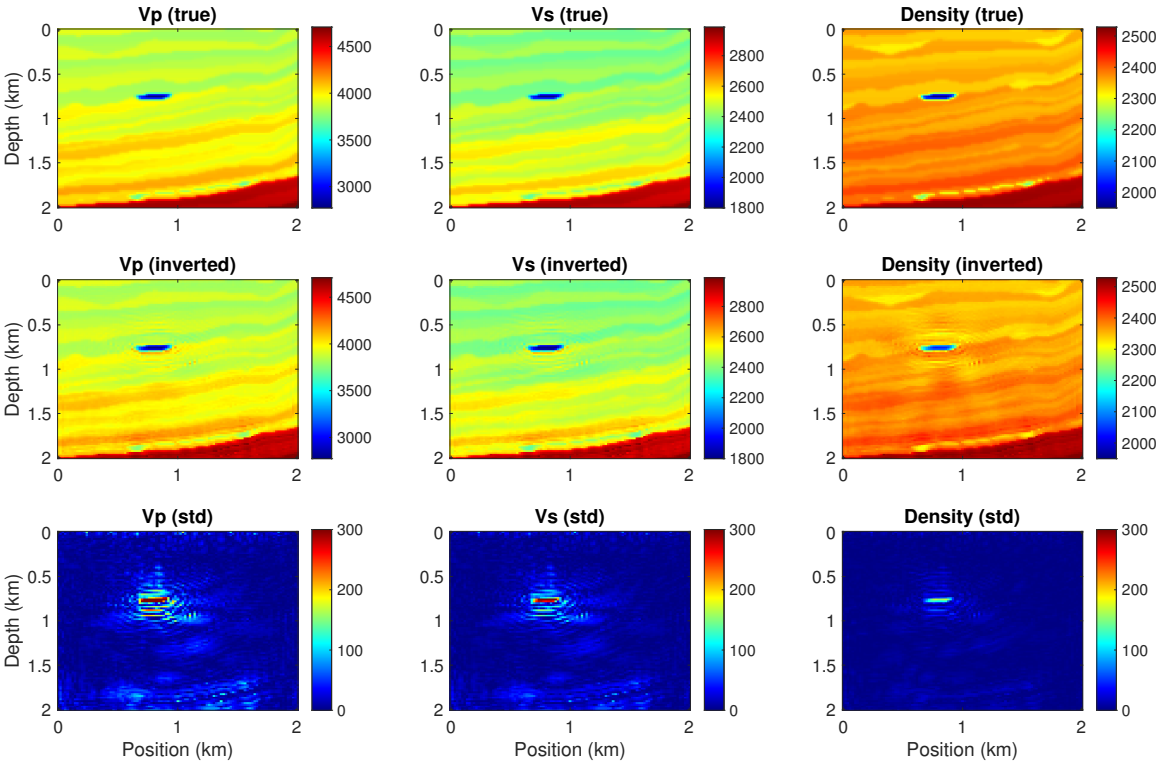

FIG. 3. Corresponding true and inverted P-wave velocity, S-wave velocity, and density models. Bottom panels: uncertainty (standard deviation) in the inverted models.

.

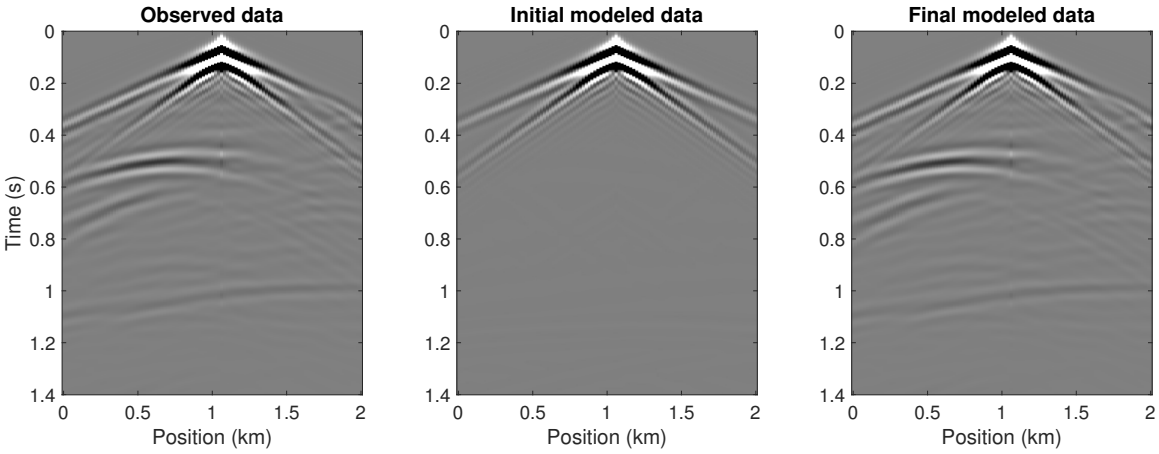

FIG. 4. Vertical components of the observed, initial, and inverted seismic data (particle velocity).

.

Time-lapse CO_2 monitoring

Next, we implement the proposed approach on a synthetic model (Figure 5) generated from the Johansen dataset (Eigestad et al., 2009; Bergmo et al., 2011). This model, derived from a simplified geometry of the original geomodel (Hu et al., 2023), highlights significantly higher porosity values in the Johansen formation compared to the overburden and underburden shales, both exhibiting very low porosity (0.1). Assuming an initial water saturation (prior to injection) of 1 throughout the model, we calculate the CO_2 saturation for the monitor survey by employing a fluid flow simulator.

In Figure 6, we compute the corresponding velocity and density models, assuming knowledge of the rock physics relation. With CO_2 replacing water, several notable changes occur. The P-wave velocity of the saturated rock decreases due to the lower bulk modulus of CO_2, while the density also decreases due to the lower density of CO_2. However, the S-wave velocity experiences a slight increase, as the fluid effect predominantly influences the density in the S-wave velocity expression. The impact of the fluid substitution is also well illustrated in the synthetic data (Figure 7). Summarizing the inversion results in Figure 8, both the porosity and CO_2 saturation models are accurately recovered, with the saturation model exhibiting relatively larger uncertainty than the porosity model. The deeper parts of these models have larger uncertainty, likely stemming from the illumination effect.

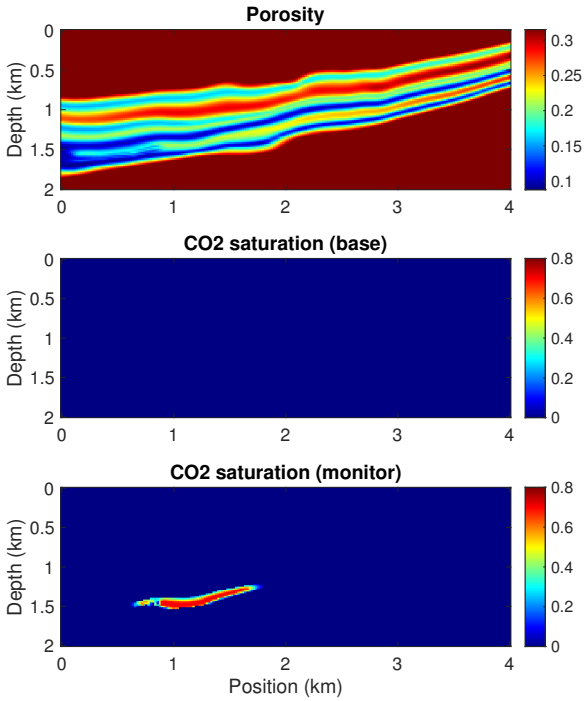

FIG. 5. True reservoir models: porosity (assuming constant in time) and CO_2 saturations before and after injection.

.

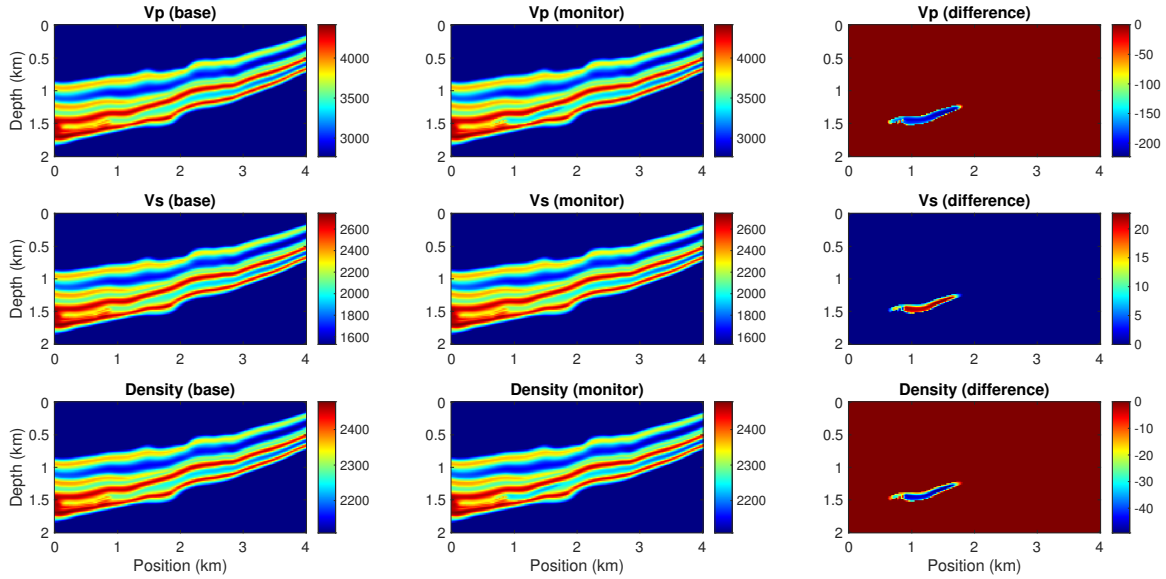

FIG. 6. True baseline, monitor, and time-lapse models of P- and S-wave velocities plus density.

.

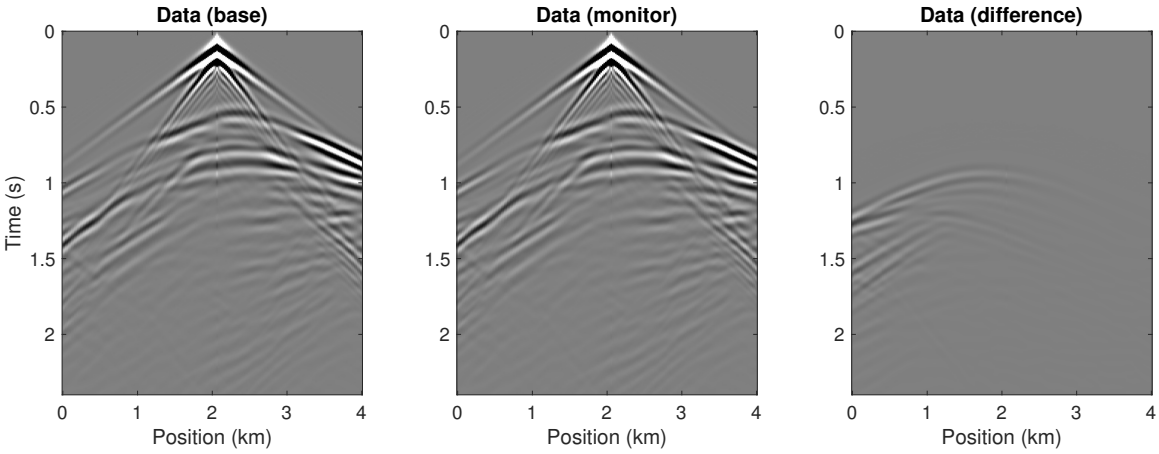

FIG. 7. Baseline, monitor, and differential seismograms computed for the true model.

.

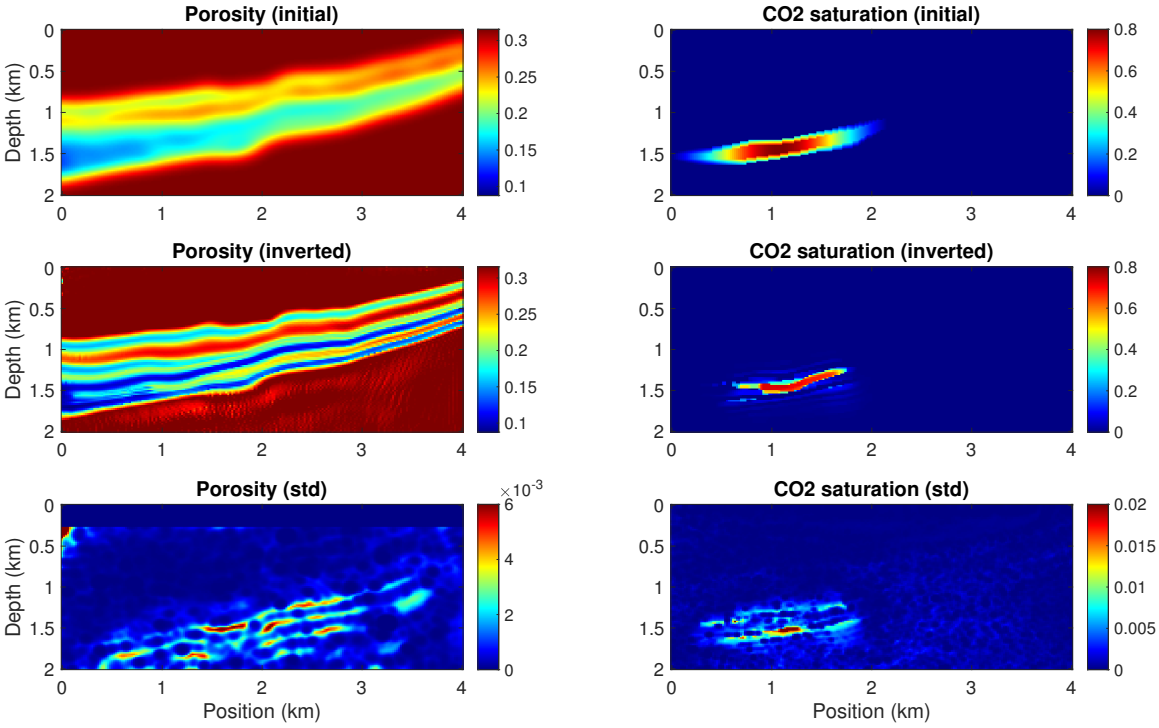

FIG. 8. Initial and inverted porosity and CO_2 saturation models. Bottom panels: uncertainty in the inverted models.

.

CONCLUSION

We formulated a multi-physics RNN-FWI approach through the integration of rock physics relations and elastic wave equations. The presented methodology offers a promising avenue for advancing seismic analysis by integrating machine learning techniques into traditional FWI frameworks. The ability to quantify uncertainties in rock physics variables enhances result interpretability, supporting more robust decision-making in subsurface exploration and monitoring.

ACKNOWLEDGMENTS

The sponsors of CREWES are gratefully thanked for continued support. This work was funded by CREWES industrial sponsors, NSERC (Natural Science and Engineering Research Council of Canada) through the grant CRDPJ 543578-19.

REFERENCES

Aki, K., and Richards, P. G., 2002, Quantitative seismology:

Bergmo, P. E. S., Grimstad, A.-A., and Lindeberg, E., 2011, Simultaneous CO_2 injection and water production to optimise aquifer storage capacity: International Journal of Greenhouse Gas Control, **5**, No. 3, 555–564.

Bosch, M., Mukerji, T., and Gonzalez, E. F., 2010, Seismic inversion for reservoir properties combining statistical rock physics and geostatistics: A review: Geophysics, **75**, No. 5, 75A165–75A176.

Bui-Thanh, T., Ghattas, O., Martin, J., and Stadler, G., 2013, A computational framework for infinite-dimensional bayesian inverse problems part i: The linearized case, with application to global seismic inversion: SIAM Journal on Scientific Computing, **35**, No. 6, A2494–A2523.

Eigestad, G. T., Dahle, H. K., Hellevang, B., Riis, F., Johansen, W. T., and Øian, E., 2009, Geological modeling and simulation of CO_2 injection in the Johansen formation: Computational Geosciences, **13**, No. 4, 435.

Gebraad, L., Boehm, C., and Fichtner, A., 2020, Bayesian elastic full-waveform inversion using Hamiltonian Monte Carlo: Journal of Geophysical Research: Solid Earth, **125**, No. 3, e2019JB018,428.

Hu, Q., Grana, D., and Innanen, K. A., 2023, Feasibility of seismic time-lapse monitoring of CO_2 with rock physics parametrized full waveform inversion: Geophysical Journal International, **233**, No. 1, 402–419.

Hu, Q., Keating, S., Innanen, K. A., and Chen, H., 2021, Direct updating of rock-physics properties using elastic full-waveform inversion: Geophysics, **86**, No. 3, MR117–MR132.

Keating, S. D., and Innanen, K. A., 2021, Null-space shuttles for targeted uncertainty analysis in full-waveform inversion: Geophysics, **86**, No. 1, R63–R76.

Liu, Q., and Peter, D., 2019, Square-root variable metric based elastic full-waveform inversion—part 2: Uncertainty estimation: Geophysical Journal International, **218**, No. 2, 1100–1120.

Mavko, G., Mukerji, T., and Dvorkin, J., 2020, The rock physics handbook: Cambridge university press.

Menke, W., 2018, Geophysical data analysis: Discrete inverse theory: Academic press.

Pratt, R. G., Shin, C., and Hick, G. J., 1998, Gauss–Newton and full Newton methods in frequency–space seismic waveform inversion: Geophysical Journal International, **133**, No. 2, 341–362.

Schuster, G. T., 2017, Seismic inversion: Society of Exploration Geophysicists.

Sen, M. K., 2006, Seismic inversion: Society of Petroleum Engineers Richardson, TX.

Sun, J., Niu, Z., Innanen, K. A., Li, J., and Trad, D. O., 2020, A theory-guided deep-learning formulation and optimization of seismic waveform inversion: Geophysics, **85**, No. 2, R87–R99.

Tarantola, A., 1986, A strategy for nonlinear elastic inversion of seismic reflection data: Geophysics, **51**, No. 10, 1893–1903.

Tarantola, A., 2005, Inverse problem theory and methods for model parameter estimation: SIAM.

Virieux, J., and Operto, S., 2009, An overview of full-waveform inversion in exploration geophysics: Geophysics, **74**, No. 6, WCC1–WCC26.

Zhang, T., Innanen, K. A., Sun, J., and Trad, D. O., 2020, Numerical analysis of a deep learning formulation of multi-parameter elastic full waveform inversion, *in* SEG International Exposition and Annual Meeting, SEG, D031S057R004.